Real-time detection of highly oxidized organosulfates and BSOA marker compounds during the F–BEACh 2014 field study

Martin Brüggemann[1,2,‡], Laurent Poulain[3], Andreas Held[4], Torsten Stelzer[1], Christoph Zuth[1], Stefanie Richters[3], Anke Mutzel[3], Dominik van Pinxteren[3], Yoshiteru Iinuma[3], Sarmite Katkevica[4], René Rabe[3], Hartmut Herrmann[3], and Thorsten Hoffmann[1]

[1]Institute of Inorganic and Analytical Chemistry, University of Mainz, Duesbergweg 10–14, 55128 Mainz, Germany
[2]Max Planck Graduate Center, Staudinger Weg 9, 55128 Mainz, Germany
[3]Leibniz-Institut für Troposphärenforschung (TROPOS), Permoserstr. 15, 04318 Leipzig, Germany
[4]University of Bayreuth, Atmospheric Chemistry, Dr.-Hans-Frisch-Straße 1–3, 95448 Bayreuth, Germany
[‡]now at: CNRS, UMR5256, IRCELYON, Institut de Recherches sur la Catalyse et l'Environnement de Lyon, Villeurbanne F-69626, France

Correspondence to: T. Hoffmann (t.hoffmann@uni-mainz.de)

Abstract. The chemical composition of organic aerosols was analyzed using complementary mass spectrometric techniques during a field study in Central Europe in July 2014 (Fichtelgebirge – Biogenic Emission and Aerosol Chemistry, F–BEACh 2014). Aerosols were analyzed in real-time by Aerosol Flowing Atmospheric-Pressure Afterglow Mass Spectrometry (AeroFAPA–MS), Aerosol Mass Spectrometry (AMS), and Chemical Ionization Atmospheric-Pressure interface Time-of-Flight Mass Spectrometry (CI–APiToF–MS). In addition, offline detection of acidic organic compounds was conducted by non-target screening of filter samples using High Resolution Mass Spectrometry (HRMS) in combination with Ultra-High Pressure Liquid Chromatography (UHPLC).

In total, 93 acidic organic compounds were identified as characteristic contributors to the organic aerosol mass at the site. Among the carbon-, hydrogen-, oxygen-containing compounds, several common biogenic secondary organic aerosol (BSOA) marker compounds were detected. High concentrations were found for the monoterpene photooxidation products 3-methyl-1,2,3-butanetricarboxylic acid (MBTCA) and 3-carboxyheptanedioic acid, suggesting that α-/β-pinene and *d*-limonene oxidation products were dominating the organic aerosol fraction. In agreement, volatile organic compound (VOC) measurements showed high mixing ratios for these monoterpenes. Moreover, the high abundance of MBTCA and 3-carboxyheptanedioic acid and their concentration ratios to earlier-generation oxidation products, such as pinic acid, indicate that aged aerosol masses were present during the campaign period. HYSPLIT trajectory calculations revealed that most of the arriving air masses traveled long distances (>1,500 km) over land with high solar radiation, further supporting this hypothesis.

Around 47% of the detected compounds from the filter sample analysis were sulfur-containing, suggesting a high anthropogenic impact on biogenic emissions and their oxidation processes. Among the sulfur-containing compounds, several organosulfates, nitroxy organosulfates, and highly oxidized organosulfates (HOOS) were unambiguously identified. In addition, correlations among HOOS classes, sulfate and highly oxidized multifunctional organic compounds (HOMs) were

investigated. The results support the hypothesis of previous studies that HOOS are formed by reactions of gas-phase HOMs with particulate sulfate. Furthermore, a good agreement was observed between HOOS formation and gas-phase peroxyradical ($RO_2^{\bullet}$) concentrations, measured by the CI–APiTOF–MS. This finding suggests $RO_2^{\bullet}$ to be either a direct or indirect precursor for HOOS. In addition, periods with high relative humidity revealed that aqueous-phase chemistry might

5   play a major role in HOOS production.

1 Introduction

Secondary organic aerosols (SOAs) are a major component of tropospheric particulate matter and known to affect the Earth's climate as well as human health (Pöschl, 2005; Baltensperger et al., 2008; Hallquist et al., 2009; Intergovernmental Panel on Climate Change, 2014; Nozière et al., 2015). In general, SOA is formed by phase transition of oxidation products

10   of volatile organic compounds (VOCs). Depending on the source of these VOCs the resulting SOA can be classified as anthropogenic SOA (ASOA), e.g. from biomass burning or fossil fuel combustion, or biogenic SOA (BSOA), e.g. from terrestrial or marine ecosystems (Hallquist et al., 2009; Nozière et al., 2015). Globally, BSOA is expected to dominate the annual mass budget of SOA to a large extent (Henze et al., 2008; Hallquist et al., 2009), although it was shown that regionally ASOA can represent the main fraction of aerosol mass (Aiken et al., 2009; Fushimi et al., 2011).

15   In the past, several marker compounds were discovered which often allow a source apportionment and, hence, a differentiation between ASOA and BSOA. As recently reported, organic acids can account for up to 51% of the OA mass in coniferous forest regions (Yatavelli et al., 2015). In agreement, common BSOA marker compounds for monoterpenes mostly comprise carboxylic acids and corresponding derivates, such as pinic acid (Yu et al., 1998; Hoffmann et al., 1998), 2-hydroxyterpenylic acid (Claeys et al., 2009) or diaterpenylic acid acetate (Iinuma et al., 2009; Yasmeen et al., 2011). These

20   oxidation products are formed by reactions of VOCs with atmospheric oxidants such as ozone, OH radicals or NO_3 radicals and are ideally characteristic for their precursor VOC. Moreover, oxidation products such as 3-methyl-1,2,3-butanetricarboxylic acid (MBTCA) are formed by photochemical oxidation of earlier-generation marker compounds, thus, allowing to trace chemical ageing of SOA in the atmosphere (Szmigielski et al., 2007; Müller et al., 2012). In addition to these solely carbon-, hydrogen-, and oxygen-containing compounds (CHO), the class of organosulfates (OS) and nitrooxy

25   organosulfates (NOS) is almost ubiquitously found in SOA particles, exhibiting supplementary marker compounds for VOC precursors. However, OS and NOS compounds might represent oxidation products of biogenic VOCs in anthropogenically influenced air masses (Zhang et al., 2009; Goldstein et al., 2009; Kristensen and Glasius, 2011). Studies have shown that OS and NOS are formed in the condensed phase, either from VOC gas-phase oxidation products with sulfuric acid in acidic sulfate aerosols (Iinuma et al., 2005; Liggio and Li, 2006; Iinuma et al., 2007; Surratt et al., 2007; Surratt et al., 2008), or

30   also directly by the reaction of gaseous SO_2 with unsaturated carboxylic acids (Shang et al., 2016). Moreover, radical mechanisms involving photochemically generated sulfate radicals might represent an additional formation pathway in aerosol particles at neutral pH (Nozière et al., 2010).

Lately a new class of monoterpene oxidation products in the gas-phase was described, named highly oxidized multifunctional organic compounds (HOMs) (sometimes also referred to as extremely low volatile organic compounds, ELVOCs) (Ehn et al., 2012; Ehn et al., 2014). These compounds exhibit O/C ratios of 0.5–1.1 and, thus, should contain several functional groups, decreasing their vapor pressures to ranges which are significantly lower than for typical BSOA

5 marker compounds (Ehn et al., 2014). Since their formation is explained by auto-oxidation processes, it is expected that multiple hydroperoxide groups are typically present per molecule (Crounse et al., 2013; Ehn et al., 2014). In agreement with this auto-oxidation hypothesis, Mutzel et al. recently showed that several HOMs contain at least one carbonyl group within their structure (Mutzel et al., 2015). Yet, until now a comprehensive structural elucidation of HOMs was not possible – neither in the gas phase nor the particle phase. Nonetheless, it is assumed that these compounds largely contribute to both

10 particle formation and growth (Riipinen et al., 2011; Donahue et al., 2012; Zhao et al., 2013, Tröstl et al., 2016).

Although the existence of HOMs was clearly demonstrated several times from gas-phase measurements (Ehn et al., 2012; Ehn et al., 2014; Rissanen et al., 2014; Jokinen et al., 2015; Mentel et al., 2015; Mutzel et al., 2015), their fate after phase transition still remains quite unclear. It has been hypothesized that due to the presence of hydroperoxide groups HOMs might participate in accretion reactions (Hallquist et al., 2009; Shiraiwa et al., 2013) or decompose via the Korcek mechanism

15 (Mutzel et al., 2015), resulting in the formation of carboxylic acids, including common BSOA marker compounds. Furthermore, from recent measurements it was speculated that the simultaneous presence of gas-phase HOMs and particulate sulfate might lead to the formation of highly oxidized organosulfates (HOOS), i.e. organosulfates with O/C ratios >1.0 (Mutzel et al., 2015). However, evidence for this hypothesis is rather unsatisfactory since it is mainly based on model calculations and offline measurements.

20 In this study, several state-of-the-art mass spectrometric techniques were used in a complementary approach to characterize the organic aerosol fraction at a rural field site in Central Europe during summer 2014. The applied techniques comprise the recently described Aerosol Flowing Atmospheric-Pressure Afterglow Mass Spectrometry (AeroFAPA–MS) (Brüggemann et al., 2015), high resolution time-of-flight Aerosol Mass Spectrometry (AMS) (Canagaratna et al., 2007), and Chemical Ionization Atmospheric-Pressure interface Time-of-Flight Mass Spectrometry (CI–APiToF–MS) (Jokinen et al., 2012).

25 Furthermore, the detection of acidic organic compounds, such as carboxylic acids and OS, was extended by non-target analysis of filter samples using High Resolution Mass Spectrometry (HRMS) in combination with Ultra-High Pressure Liquid Chromatography (UHPLC). Besides the detection and identification of common BSOA marker compounds, the formation of HOOS and their correlation to HOMs was investigated using online and offline instrumentation.

2 Experimental

30 ### 2.1 Field Site Description

All measurements were conducted in July 2014 (15th–27th) during the F–BEACh 2014 (Fichtelgebirge - Biogenic Emissions and Aerosol Chemistry) field campaign. The measurement site was located in a rural area at an altitude of 766 m a.s.l. in the

Fichtelgebirge mountain range in Southeast Germany (BayCEER Waldstein-Pflanzgarten, 50°08'35" N, 11°51'49" E, operated by the University of Bayreuth). The site is surrounded by a mostly coniferous forest which is dominated by Norway spruce (~90%). A mixture of larch, beech, maple, and pine accounts for the rest of the tree population (Staudt and Foken, 2007).

2.2 AeroFAPA–MS Measurements

The AeroFAPA ion source was used in combination with an ion trap mass spectrometer (LCQ Deca XP Plus, Thermo, San José, CA, USA) for real-time analysis of ambient organic aerosol particles. Since a detailed description of the technique can be found elsewhere (Brüggemann et al., 2015), only a brief description will be given here.

In general, AeroFAPA–MS is a soft-ionization technique which allows the online detection of organic compounds in aerosol particles. The negative mode, which was applied throughout the field study, is selective towards acidic compounds, such as carboxylic acids and (nitrooxy) organosulfates. For the analysis, aerosol particles were drawn from a height of ~4 m above ground into the manifold of the AeroFAPA at a flow rate of 0.9 L min^{-1}. Before reaching the AeroFAPA–MS, the aerosol stream passed an activated charcoal denuder in order to remove gaseous species from the aerosol sample. Evaporation of organic aerosol components prior to ionization was ensured by heating the inlet to 200 °C. A helium glow discharge plasma was used to generate excited helium atoms and primary reagent ions which ionized the compounds of interest in the so-called afterglow region. During the campaign, a current of 55 mA was used, resulting in a discharge voltage of ~400 V. In addition, a potential of –15 V was applied to the exit capillary of the AeroFAPA to enhance ion transmission. The resulting analyte ions, typically [M–H]$^-$, were then sampled and detected by the mass spectrometer. A voltage of –15 V was applied to the mass spectrometer inlet capillary, equaling the potential of the AeroFAPA's exit capillary. The tube lens was held at 0 V. All mass spectra were recorded in automatic gain-control mode with 300 microscans spectrum^{-1}, giving roughly one full scan mass spectrum (m/z 130–500) per minute. The maximum ion trap injection time was set to 200 ms. MS^{n} experiments were performed to elucidate the structure of the detected compounds. Data were recorded using XCalibur 2.0.7. Background subtraction of the acquired mass spectra was conducted by measuring a blank sample for half an hour every day. For the subsequent data analysis all files were converted to text files and analyzed using Matlab (R2014b, Mathworks Inc., USA). In order to compare and correlate data from different instruments a unified time vector was created with time intervals of 10 minutes. Thus, all signals, except the filter sample data, are average values for 10 minutes.

2.3 AMS Measurements

A High Resolution Time-of-Flight Aerosol Mass Spectrometer (HR–ToF–AMS, Aerodyne, USA, Canagaratna et al., 2007), was used to measure the submicron mass concentrations and size distributions of non-refractory particulate organic matter, sulfate, nitrate, ammonium and chloride. The AMS was located in an adjacent laboratory container and connected to a sampling line with a PM$_{10}$ inlet located at ~6 m above ground level. Relative humidity on the sampling line was maintained below 35% using a Nafion® dryer. A chemical dependent collection efficiency (CDCE) was applied on the AMS data

according to Middlebrook et al. (2012). The data quality insurance of the AMS results was made by successfully comparing the mass closure of the PM_1 aerosol chemical mass concentration as measured by the AMS to the estimated mass concentration measured by the T-SMPS as previously described in Poulain et al. (2014).

2.4 CI–APiTOF–MS Measurements

5   Gas-phase concentrations of HOMs and sulfuric acid were measured using a CI–APiTOF–MS (chemical ionization atmospheric-pressure interface time-of-flight mass spectrometer). A detailed description of the instrument can be found elsewhere (Jokinen et al., 2012; Mutzel et al., 2015). Briefly, an ^{241}Am source was used to produce nitrate ions which were electrostatically guided into the sample flow to give nitrate clusters with gas-phase compounds present in the sampled air. Then, the resulting clusters were transferred into the high vacuum region and detected by TOF-MS. Calibration of the

10   instrument was performed using sulfuric acid (m/z 96.9601, HSO_4^-).

2.5 T-SMPS Measurements

Particle number size distributions were measured with a twin scanning mobility particle sizer (SMPS) custom-built by TROPOS (Leipzig, Germany) according to the design recommended by Wiedensohler et al. (2012). The instrument includes membrane dryers to keep the relative humidity below 40% both in the sample and the sheath flow. The aerosol sample is

15   brought to bipolar charge equilibrium using a commercial ^{85}Kr neutralizer and sent to a Hauke-type differential mobility analyzer (DMA). The mobility diameter range from 10 nm to 710 nm was scanned in 71 size bins with a time resolution of 5 min. The closed-loop sheath flow rate was set to 5 L min^{-1} while the sample flow was directed to a Model 3772 condensation particle counter (TSI Inc., Shoreview, Minnesota, USA) for particle detection with a flow rate of 1 L min^{-1}.

2.6 VOC measurements

20   VOCs were actively sampled on commercial two-stage cartridges filled with Tenax TA/Carbograph 5TD (Markes International, Cincinnati, Ohio, USA) for 30 min with a flow rate of 0.1 L min^{-1} in and above the spruce canopy at 12 m and 31 m above ground level for subsequent offline gas chromatographic analysis. Samples were taken during daytime from 09:00 to 20:00 (CET) on four selected days during F–BEACh 2014. Ozone scrubbers coated with potassium iodide were used to minimize oxidation of collected compounds. After sampling, the cartridges were sealed immediately with metal caps,

25   placed in a screw-cap PTFE container and kept refrigerated until analysis.

In the laboratory, VOCs were analyzed using standard thermal desorption gas chromatography with flame ionization detection (TD–GC–FID). The sample cartridges were thermally desorbed (200 °C), pre-focused on a Peltier-cooled trap (–15 °C), injected onto an Rxi-5ms column (30 m, 0.32 mm, 1.00 µm, Restek, Bad Homburg, Germany) in a Sichromat 1 (Siemens AG, Germany) gas chromatograph, and quantified by flame ionization detection.

2.7 Filter Sample Analysis Using UHPLC–(-)ESI–HRMS

Filter samples were taken twice a day by passing an air flow of 27.5 L min^{-1} from ~6 m above ground (PM$_{2.5}$) through tetrafluorethylene-coated borosilicate filters (70 mm, Pallflex T60A20, Pall Life Science, USA). The sampling time was ~8 hours for daytime filters (9 a.m.–5 p.m.) and ~16 hours for nighttime filters (5 p.m.–9 a.m.). After sampling, the filters

5   were stored at <-18 °C until analysis. Blank filters were taken every 2 to 3 days by placing a filter into the filter holder for ~20 min without sample flow.

For the extraction procedure one half of a filter sample was cut into pieces and 1.5 mL of a methanol/water solution (9:1) were added as extracting agent. Then, the sample was sonicated for 30 min. The extract was transferred into a separate glass vial and the filter sample extracted three more times in the same way. The combined extracts were then evaporated to

10   dryness under a gentle stream of nitrogen at 50 °C. Afterwards, the residue was dissolved in 200 µL using a solution of acetonitrile/water (2:8). To compensate for losses during the evaporation step, an average recovery rate was determined for pinic acid, which served as a surrogate for the quantification of other monoterpene oxidation products. Here, an average recovery rate of 85% was found and applied to the detected organic compounds.

For the LC separation of the filter extracts a UHPLC system (Dionex UltiMate 3000, Thermo Scientific, Germany) equipped

15   with a Hypersil Gold column (C18, 50x2.0 mm, 1.9 µm, Thermo Scientific, Germany) was used. The injection volume was 20 µL per run and each sample was measured in triplicate. As eluents served solutions of ultrapure water with 2% acetonitrile and 0.04% formic acid (eluent A) and a solution of acetonitrile with 2% of ultrapure water (eluent B). At a flow rate of 500 µL min^{-1} the following gradient was used to optimize the separation: 5% B at 0.00 min, 5% B at 0.50 min, 20% B at 1.00 min, 20% B at 1.50 min, 90% B at 2.00 min, 90% B at 4.00 min, 5% B at 4.05 min, and 5% B at 4.10 min.

20   The UHPLC system was coupled to a Q-Exactive mass spectrometer (Thermo Scientific, Germany) which was used to obtain high resolution mass spectra (resolving power of R=7·10^4 at m/z 200). Ionization of the LC eluent was carried out using electrospray ionization (ESI) in the negative mode with 40 psi sheath gas (N$_2$) and 20 psi aux gas (N$_2$). The capillary temperature was set to 350 °C and a potential of –3.0 kV was applied to the ESI needle. During each LC run the mass spectrometer operated in full scan mode with a scan range of m/z 80–550. Before running the measurements, the instrument

25   was calibrated using the Pierce^{TM} calibration solution (Thermo Scientific, USA). For an accurate calibration of the lower mass range, butyric acid was added to the solution.

The obtained LC–MS data were recorded by XCalibur 2.2 (Thermo Scientific, USA) and further analyzed by Sieve 2.2 (Thermo Scientific, USA) which allowed a non-target screening of the obtained data set. The threshold for signal abundance was set to 2.5·10^6 a.u. for the detection of significant signals in the obtained chromatograms after background subtraction by

30   the software. For the elemental formula assignments the following isotopes and conditions were used: ^{12}C (0–50), ^{1}H (0–100), ^{16}O (0–40), ^{14}N (0–4) and ^{32}S (0–4). The mass tolerance was set to ±5 ppm. Afterwards, the obtained compound list was checked for chemically unreasonable formula assignments, such as the absence of hydrogen in carbon-containing compounds or impossible O/C ratios (O/C < 3; 0.1 < H/C < 6).

3 Results and Discussion

3.1 Detection of acidic oxidation products in SOA particles using online and offline mass spectrometry

In total, the automated non-target analysis of the filter samples by LC–MS resulted in 695 compounds which showed significant signal intensities after background subtraction. From this large number of compounds only those compounds were selected for the subsequent analysis which had a formula assignment within a mass accuracy range of ± 5 ppm and showed an integrated peak area of $>10^7$ a.u. for at least two separate filter samples. Eventually, these thresholds led to 93 compounds which were identified from the data analysis (Fig. 1 and Supplemental Material). In general, the entire group of CHO compounds can be assigned to the class of organic acids since all measurements were carried out in the negative ion mode which is selective towards acidic compounds. Among the identified organic acids several common biogenic SOA marker compounds were detected, such as pinic acid (m/z 185.0819, $[M–H]^-$) (Yasmeen et al., 2011) or terpenylic acid (m/z 171.0663, $[M–H]^-$) (Claeys et al., 2009). The concentrations of these marker compounds in $PM_{2.5}$ were estimated using pinic acid as calibration standard. Despite similar chemical structures, the ionization efficiencies might, however, differ to a certain extent among these marker compounds. For example, in a post-calibration experiment the response of the MS for MBTCA was found to be ~80% of the one for pinic acid. Therefore, the given values should rather be taken as semi-quantitative, and in the case of MBTCA considered as a lower limit. Table 1 gives an overview of the identified marker compounds and their average concentrations during the campaign period. A comprehensive list of all detected compounds is given in the Supplemental Material.

The most dominant marker compounds during the campaign period were MBTCA and 3-carboxyheptanedioic acid with estimated concentrations of 13.8 ($\pm$ 9.0) ng·m^{-3} and 10.2 ($\pm$ 6.6) ng·m^{-3}, respectively. While MBTCA depicts a later-generation oxidation product of α-/β-pinene (Szmigielski et al., 2007; Müller et al., 2012), 3-carboxyheptanedioic acid is a major oxidation product of d-limonene (Jaoui et al., 2006). These findings suggest that the site was strongly influenced by biogenic emissions consisting mainly of α-/β-pinene and d-limonene and their corresponding oxidation products. This hypothesis is further supported by monoterpene measurements which showed relative mixing ratios of 38% α-pinene, 23% β-pinene, 19% d-limonene, 12% Δ-3-carene and 8% camphene. The median mixing ratios of the sum of these five monoterpenes were 0.8 ppb$_V$ above the canopy and 1.6 ppb$_V$ within the canopy. In addition, from a comparison with the MEGAN emission model (Guenther et al., 2012), the five monoterpenes α-/β-pinene, d-limonene, Δ-3-carene, and camphene are estimated to contribute about 80% to the total monoterpene emissions at the F–BEACh site.

Despite the high mixing ratios for monoterpenes, rather low abundances were found for early-generation oxidation products, e.g. pinic acid ($c = 4.7$ ($\pm$ 2.5) ng·m^{-3}). However, since MBTCA as well as 3-carboxyheptanedioic acid are known to be formed via photooxidation of their monoterpene precursors (Szmigielski et al., 2007; Jaoui et al., 2006), this observation might indicate the occurrence of fast photochemical aging processes, eventually resulting in high abundances for these compounds during the campaign period. Besides several monoterpene oxidation products, also a marker compound for sesquiterpene oxidation, i.e. β-nocaryophyllinic acid, could be identified (van Eijck et al., 2013). However, since

sesquiterpene oxidation products require specialized setups for detection because of their high reactivity and low volatility, the contribution of sesquiterpene oxidation products on particle composition cannot be quantified here.

As can be seen from Fig. 1, several sulfur and nitrogen-containing compounds were found on the filter samples, i.e. CHOS, CHON, and CHONS. Similar to the CHO group, all these compounds have to exhibit a certain acidity which allows the detection as $[M–H]^-$ ions in the negative ion mode. Therefore, the CHOS and CHONS compounds were assigned to organosulfates and nitrooxy organosulfates, respectively, which contain an acidic organic sulfate ($R–OSO_3H$) functionality. The CHON group might possibly comprise acidic organonitrates, although, no further evidence can be given here. While only 4% of the compounds were classified as CHON compounds about 47% of the compounds are either belonging to the CHOS or the CHONS group. This large number of organosulfates and nitrooxy organosulfates is, however, not surprising since these compound classes are ubiquitously found in organic aerosol particles and readily accessible for deprotonation via electrospray ionization (Hallquist et al., 2009; Nozière et al., 2015). A comprehensive list of all sulfur- and nitrogen-containing compounds is given in the Supplemental Material.

Several of the identified sulfur-containing compounds were already studied in the past and found in field and laboratory studies (Surratt et al., 2008; Altieri et al., 2009; Nguyen et al., 2012; Lin et al., 2012). In general, it is assumed that organosulfates and nitrooxy organosulfates have a mixed biogenic/anthropogenic origin, possibly involving particulate sulfuric acid, SO_2, NO_X and radical-initiated chemistry (Surratt et al., 2008; Zhang et al., 2009; Nozière et al., 2015). As can be seen from Table 2, among the CHOS compounds several highly oxidized organosulfates (HOOS) were found on the filter samples. This recently described compound class exhibits O/C ratios greater than 1.0 and is possibly connected to the presence of gas-phase HOMs and, thus, might have implications for new particle formation processes (Ehn et al., 2014; Mutzel et al., 2015).

Real-time analysis of aerosol particles reaching the site was carried out using a HR–ToF–AMS and the recently described AeroFAPA–MS (Brüggemann et al., 2015). While the AMS was used for a general classification of the aerosol particles' components in ammonium, sulfate, nitrate, chloride and organics, the AeroFAPA–MS was resolving the organic fraction on a molecular level. In summary, the majority of the aerosol particle mass was classified as organic compounds (63.4%), followed by sulfate (21.1%), ammonium (8.7%) and nitrate (6.7%).

Figures 2 and 3 show the concentrations of organics, measured by the AMS, in comparison to the total ion current (TIC) measured by the AeroFAPA–MS. It is assumed that the TIC, i.e. the sum of all detected ions, only shows signals for organic compounds since inorganic species are typically not volatilized and ionized by the AeroFAPA ion source. Additionally, the particle number size distributions and the main directions of 96 hours backward trajectories, calculated by HYSPLIT (HYbrid Single-Particle Lagrangian Integrated Trajectory; Draxler and Rolph, 2013), are given for the campaign period. As can be seen from Figure 2, the signals for the 93 identified compounds by LC–HRMS and the signals of AeroFAPA–MS generally follow the same trends and are in agreement with the trend for the total organic aerosol mass, measured by the AMS. All three instruments show a maximum of signal intensities during the night of the 21st of July which can be explained by particles with relatively large diameters (median diameter ~150 nm) from regional sources reaching the site. For the

organic aerosol fraction a maximum concentration of 16.9 µg·m⁻³ was determined by the AMS for this period. The days before the 21ˢᵗ of July are mainly characterized by trajectories coming from Western Europe and Northern Germany while afterwards the trajectories are arriving almost exclusively from Eastern and Northeastern Europe, i.e. Estonia and Russia.

Deviations between the signals of the instruments are mostly observed during nighttime which is possibly due to the formation of non-acidic compounds, such as alcohols, aldehydes, or ketones, possibly formed by nighttime nitrate radical chemistry, eluding detection by AeroFAPA–MS. In contrast, compounds containing organic bonded sulfate, such as organosulfates or nitroxy organosulfates, are readily measured by the AeroFAPA–MS and LC–HRMS, however, the AMS cannot differentiate between inorganic sulfate and organic bonded sulfate. The same bias is typically observed for measurements of inorganic nitrate and organonitrates. Thus, all sulfate and nitrate signals of the AMS were assigned to the inorganic fraction, possibly leading to an underestimation of the organic aerosol mass (Liggio and Li, 2006; Farmer et al., 2010).

In order to quantify the portion of organic compounds in aerosol particles that was measureable by AeroFAPA–MS, the signals of AMS organics and the TIC of the AeroFAPA–MS were plotted against each other. As depicted in Fig. 3 (panel a), the data of the two instruments exhibit a linear correlation for the entire campaign period. By calculation of a linear regression fit a correlation coefficient of $R^2 = 0.83$ was determined, indicating that about 83% of the variability of the organic aerosol mass can be explained by the AeroFAPA–MS signals. Furthermore, the AeroFAPA–MS signals ([M–H]⁻) of the 93 compounds that were unambiguously identified as major contributors to the organic aerosol fraction from the filter sample analysis, were plotted as a function of the organic aerosol mass, determined by the AMS (Fig. 3, panel b). Similar to the correlation of the TIC of the AeroFAPA–MS to organic aerosol mass, a linear correlation was found. Interestingly, about 80% ($R^2 = 0.80$) of the organic aerosol's variability can be explained by these signals, supporting the hypothesis that these compounds reflect major sources of the organic aerosol mass at the site. Nonetheless, it should be noted that from the AeroFAPA–MS data an unambiguous formula assignment is not possible due to the unit mass resolution.

Figure 4 (panel a) shows the summed AeroFAPA-MS mass spectra over the entire measurement period. As can be seen from this figure, the AeroFAPA–MS spectra support the aforementioned hypothesis that the composition of the particle phase reaching the site were dominated by BSOA marker compounds such as 2-hydroxyterpenylic acid (*m/z* 187, [M–H]⁻), MBTCA and 3-carboxyheptanedioic acid (both *m/z* 203, [M–H]⁻). Moreover, signals for pinonic acid (*m/z* 183, [M–H]⁻) and pinic acid (*m/z* 185, [M–H]⁻) remain quite low over the entire campaign period, as it was already observed for the filter samples, confirming the already mentioned low concentration of primary oxidation products at the sampling site. The ratio of signals for MBTCA and pinic acid, which can be used as aging proxy for organic aerosols, shows an average value of 5.76, however, even ratios of >32 were observed for single days (Supplemental Material Fig. S-7). Although this ratio is very specific for the instrumental setup of the AeroFAPA–MS and its ionization mechanisms, these extremely high values suggest that mainly air masses with aged aerosol reached the site. In agreement, HYSPLIT trajectory calculations reveal that arriving air masses typically traveled several days over land with distances of >1,500 km at low altitudes (Figures S-1 to S-6). Moreover, the majority of the trajectories are accompanied by high solar radiation without any precipitation along their way,

leading to a high degree of solar radiation and, therefore, photochemical processing of the transported aerosol masses (see Supplemental Material). Since MBTCA exhibits a rather long atmospheric lifetime of ~10 days (Nozière et al., 2015), the observed high abundance of MBTCA might, therefore, not be solely the result of rapid photochemically-driven oxidation near the sampling site, but could be influenced to a certain extent by long range transport of organic aerosols. It should also

5 be noted that there are two trajectories (20th and 21st of July, Figure S-1) travelling along the Czech/German border mostly over coniferous forest for at least 24 h before arriving at the Waldstein site. Previously, these southeasterly wind directions have been related to regional new particle formation events observed at the site (Held et al., 2004).

In general, most acidic monoterpene oxidation products show odd m/z ratios in the mass spectra of the AeroFAPA–MS, since they only contain carbon, hydrogen and oxygen atoms and are detected as [M–H]$^-$ ions. However, the sum of

10 AeroFAPA–MS spectra also exhibits elevated signals at even m/z ratios, such as m/z 308, showing a high linear correlation (R^2=0.76) to the organic aerosol mass measured by the AMS (Fig. 4, panel b). According to the nitrogen rule, these signals correspond to nitrogen-containing compounds with an odd number of nitrogen atoms. To identify this compound, the LC–MS data were checked for signals at the nominal m/z ratio 308. In fact, a nitrogen-containing compound with the chemical formula $C_{11}H_{18}O_9N$ (m/z 308.0987, [M–H]$^-$) was detected from the filter analysis at this nominal m/z ratio. Since the

15 AeroFAPA–MS as well as the LC–ESI–MS are selective towards acidic compounds, this signal possibly indicates the presence of a highly oxidized nitrogen-containing carboxylic acid, such as a nitrooxy carboxylic acid. Similarly, a signal at m/z 250 is found in the AeroFAPA–MS spectra, showing a linear correlation to the AMS data. In this case, however, the signals of the LC–MS analysis exhibited quite low abundances. Nonetheless, one significant signal was identified at m/z 250.0208, representing $C_7H_8O_9N$ ([M–H]$^-$). Due to the high oxygen content of these two compounds and their low

20 corresponding signals from the LC–MS analysis, it is assumed that they possibly decompose during sampling, transport, storage or processing of the filter samples. Moreover, nitrooxy compounds are also known to be prone to nucleophilic substitution by SO_4^{2-}, forming the more stable organosulfate derivates (Darer et al., 2011). Thus, only online detection methods such as AeroFAPA–MS would allow a reliable detection of such highly oxidized nitrooxy carboxylic acids in organic aerosols. Nonetheless, different ionization efficiencies might also have a significant effect on the detection of these

25 compounds and could explain the observed deviations to a certain degree.

3.2 Real-time detection of HOOS in the field

In order to investigate the presence of HOOS using real-time data of the AeroFAPA–MS, four representative compounds were chosen which were previously identified from the filter analysis (Table 2). The selection procedure for these representative compounds was based on the following criteria: Firstly, the HOOS were grouped according to their number of

30 carbon atoms per molecule into C7 to C10 compounds. Secondly, since the AeroFAPA–MS exhibits only unit mass resolution the signals of the representative HOOS had to show a higher intensity on their nominal m/z ratio than any other signal for the LC–MS data. Moreover, special care was taken that no HOOS with identical nominal m/z ratios but different

carbon chain lengths were chosen as representative, as it is the case e.g. for $C_9H_{13}O_9S$ and $C_{10}H_{17}O_8S$ (both at nominal m/z 297). Eventually, the high mass resolution data of the LC–MS analysis were checked for HOOS that meet these criteria.

As can be seen in Fig. 5, for each of the HOOS classes one appropriate compound was found. For the C7 HOOS the signal at m/z 239.0231 was chosen, representing $C_7H_{11}O_7S$ ([M–H]$^-$). This signal shows the highest abundance of all HOOS compounds from the filter measurements, as it was already observed by Mutzel et al. (2015), and almost no other signal was detected in significant abundances at this nominal m/z ratio. For the C9 HOOS an intense signal at m/z 267.0543 ($C_9H_{15}O_7S$, [M–H]$^-$) met the criteria and was selected. In agreement, the C7 and C9 HOOS have also been identified before in laboratory and field studies by Surratt et al. (2008). The m/z ratio at 285.0284, embodying $C_8H_{13}O_9S$ ([M–H]$^-$), was chosen as representative for the C8 HOOS. Here, it should be noted that this signal was observed in lower abundances and some additional, but less distinct, signals were found at this nominal m/z ratio. A similar case was observed for the C10 HOOS for which the signal at m/z 327.0390 ($C_{10}H_{15}O_{10}S$, [M–H]$^-$) was chosen as representative. In general, for all of the selected compounds it was assumed that additional minor signals on the same nominal m/z ratio have negligible effects on the overall signal intensity for HOOS over the entire measurement period. Furthermore, it was assumed that AeroFAPA–MS detects the selected HOOS as [M–H]$^-$ ions, and thus, at the same nominal m/z ratio as for the LC–MS data. A comparison between the time traces of HOOS detected by LC–MS and AeroFAPA–MS is given in the Supplemental Material (Fig. S-10), showing similar trends for the two techniques and supporting the suitability of the selected criteria.

Figure 6 (panel a) depicts the signals for HOOS of the AeroFAPA–MS which were plotted as a function of each other and checked for linear correlations among them. In addition, the particulate sulfate concentrations and relative humidity (RH) are given by the marker size and the color code, respectively. In general, all four HOOS classes show a linear correlation to each other, suggesting similar sources for these compounds. However, the group of C7 HOOS exhibits significant lower correlation coefficients of 0.51, 0.55 and 0.52 to the C8, C9, and C10 HOOS, respectively. This decreased correlation might indicate that the source for the C7 class is somewhat different to the larger HOOS. In fact, while the signal for $C_7H_{11}O_7S^-$ (m/z 239.0231, [M–H]$^-$) shows the highest abundances of all HOOS from the filter sample analysis, as it was also reported by Mutzel et al. (2015), the AeroFAPA–MS measurements exhibit only low signals for this compound, further suggesting a different source than for the other HOOS. Possibly, this compound is a decomposition product of the larger HOOS compounds and is formed over time on the filter surface during sampling, storage and/or processing of the sample. This hypothesis is further supported by comparing time traces for HOOS on single days where the signals for the larger HOOS classes differ clearly from the signals for the C7 HOOS (Supplemental Material Fig. S-8).

As can be seen from Figure 6, all HOOS classes yield the strongest signals for high particulate sulfate concentrations, however, no linear correlation could be observed over the entire campaign period except for single days. Moreover, the most intense signals for HOOS were observed during high RH periods which coincided with a strong increase of the particulate sulfate concentrations, following the same trend as for the HOOS signals (Fig. 6, panel b). This finding might suggest that aqueous-phase chemistry plays a major role for HOOS production, as it is known for other OS compounds (Herrmann et al., 2015).

In particular, during the high RH period from 21st–23rd of July, the sulfate concentrations and signals for HOOS show a linear correlation (R^2=0.70). Figure 6 (panel b) depicts the time trace of the signals for the HOOS and the particulate sulfate concentrations. Additionally, the RH is given by the color code. Within the first hours of July 21st the signals for HOOS and the sulfate concentrations still show some minor deviation, however, starting roughly from 9 a.m. both time traces follow

5   almost exactly the same trend for the rest of this period, for which RH values mostly exceed 80%. During such high RH periods dissolved HSO_4^- might react with HOMs after phase transition via a nucleophilic attack to give HOOS, as it was already proposed previously (Mutzel et al., 2015). Moreover, the required rapid phase transition of gas-phase HOMs into the particle phase is further supported by the observed trend for the sum of HOMs, measured by the CI–APiTOF–MS. As depicted in the figure, until ~11 a.m. of July 22nd the RH values are rather high (RH > 60%). During this period, i.e. ~6 p.m.

10   of 21st to ~11 a.m. of the 22nd of July, the signal for gas-phase HOMs is hardly correlated to neither the HOOS signal nor the sulfate concentration and shows rather low abundances. However, as soon as the RH decreases to values below 60%, the gas-phase concentration of HOMs exhibits an immediate and strong increase, roughly tripling the sum of HOMs within ~1.5 hours. It should be noted that some strong precipitation around midnight of the 21st of July led to the observed strong decrease in particulate sulfate as well as HOOS concentrations.

15   In order to further investigate the formation of HOOS and the role of possible precursor HOMs, single m/z ratios of the CI–APiTOF–MS were analyzed in more detail for the 17th and 24th of July. Since during the high RH periods the gas-phase concentrations of HOMs were extremely low due to a rapid phase transition (Figure 7, panel b), only these two days with low RH values were chosen for a further data analysis and discussion. In general, during dryer periods, signals with an odd m/z ratio in the mass spectra of the CI–APiTOF–MS dominate the sum of gas-phase HOMs (see Supplemental Material Fig.

20   S-11). As it was reported previously (Ehn et al., 2014; Jokinen et al., 2014), several of these compounds represent peroxyradicals ($RO_2^\bullet$) which may act as precursors for closed-shell HOMs. Remarkably, the signals for $RO_2^\bullet$ and HOOS follow the same trends during the dry periods, possibly revealing a connection between these species. As an example Fig. 7 (panel a) depicts the time traces of a C10 HOOS (m/z 327, $C_{10}H_{15}O_{10}S$, $[M–H]^-$) and the most abundant $RO_2^\bullet$, i.e. $C_{10}H_{15}O_8^\bullet$ (m/z 325, $[M+NO_3]^-$), which might represent a possible precursor species for this HOOS compound. In addition, the gas-

25   phase concentration of H_2SO_4 (divided by 4) and RH are given. As can be seen for July 17th and 24th the signal for $RO_2^\bullet$ is increasing with time, showing its maximum at ~$4 \cdot 10^6$ molecules cm^{-3} for both days around 11 a.m., and is afterwards slowly decreasing again. In each case, the signal for the C10 HOOS follows almost exactly the concentration of the $RO_2^\bullet$. Therefore, $RO_2^\bullet$ might represent either a direct, or at least indirect, precursor for HOOS. Since it can be assumed that not only closed-shell HOMs contain carbonyl-functionalities, as it was recently shown (Mutzel et al., 2015), but also their corresponding

30   precursor $RO_2^\bullet$, a nucleophilic attack by HSO_4^- is in any case possible and might explain HOOS formation either in the particle-phase or even by a humidity-dependent reactive uptake, as it is known e.g. for trace gases such as N_2O_5 or H_2O_2 (Kolb et al., 2010).

For both days also a significant amount of gas-phase H_2SO_4 was present, showing maximum values of ~$1.6 \cdot 10^7$ molecules cm^{-3} and ~$1.3 \cdot 10^7$ molecules cm^{-3} for July 17th and 24th, respectively. It should be noted that in contrast

the particulate sulfate concentration was rather high during July 17th (maximum at ~5.7 µg m^{-3}) but quite low for July 24th (maximum at ~2.8 µg m^{-3}). In principle, gas-phase H_2SO_4, which gets rapidly dissolved in the aqueous phase during high RH periods, might present an additional sulfur source for HOOS generation during such dryer periods. However, correlations during the campaign period were only observed for single days when high HOOS signals coincided with

5   elevated gas-phase H_2SO_4 concentrations (Fig. 7, panel b). Thus, due to the limited data set and ambient conditions the exact reaction mechanisms for HOMs and HOOS cannot be discriminated here. In general, it can also be expected that the presence of precursor HOMs is the rate-limiting step in HOOS production, since concentrations for particulate sulfate as well as gas-phase H_2SO_4 are typically significantly higher. The afore-mentioned reaction mechanisms for the high RH periods, i.e. nucleophilic attack by HSO_4^- might, therefore, still play an important role for the dryer periods.

10   **4 Conclusions**

The chemical composition of the organic aerosol fraction was analyzed during the F–BEACh 2014 campaign with complementary mass spectrometric techniques. The non-target analysis of filter samples by UHPLC–ESI–HRMS revealed 93 acidic organic compounds which are characteristic for major sources of the organic aerosol mass at the site. In addition, it was shown that around 47% of the identified compounds were sulfur-containing, suggesting a rather high anthropogenic

15   impact on biogenic emissions and their oxidation processes. Among the sulfur-containing compounds, several OS, NOS, and HOOS were unambiguously identified. The CHO-containing compounds exhibited several common BSOA marker compounds, showing rather high concentrations for the monoterpene photo-oxidation products MBTCA and 3-carboxyheptanedioic acid. This finding suggests that aerosol masses reaching the site were mostly dominated by α-/β- pinene and d-limonene oxidation products. In agreement, VOC measurements showed high mixing ratios for these

20   monoterpenes in and above canopy level. Furthermore, the abundance of MBTCA and 3-carboxyheptanedioic acid and their ratios to earlier-generation oxidation products, such as pinic acid, suggest that air masses containing relatively aged aerosol masses were present during the campaign period. In agreement, HYSPLIT trajectories revealed that most of the air masses traveled long distances (>1,500 km) over land with high solar radiation.

In general, real-time measurements of the aerosol constituents using AeroFAPA–MS, AMS and CI–APiToF–MS further

25   supported these findings. Additionally, correlations among HOOS classes, sulfate and gas-phase HOMs were investigated. In agreement with previous studies the results support the hypothesis that HOOS are formed by reactions of gas-phase HOMs with particulate sulfate, i.e. HSO_4^- (Mutzel et al., 2015). Since the signals for the C7 HOOS show rather low abundances and only low correlations to the other HOOS it is assumed that these HOOS might represent decomposition products of larger HOOS. This finding is, however, not contradicting previous publications which found the highest concentrations for C7

30   HOOS from the analysis of filter samples (Mutzel et al., 2015). It is rather suggesting that larger HOOS decompose not only in the atmosphere but also during filter sampling, storage or processing, forming the observed C7 decomposition products. Furthermore, gas-phase $RO_2^•$ are assumed to be precursors for HOOS since a good agreement was found between HOOS

formation and RO$_2^{\bullet}$ concentration during dry periods. High RH periods, however, revealed that aqueous-phase chemistry is presumably playing a major role in HOOS production since the highest HOOS signals coincided with high RH values and high particulate sulfate concentrations.

5 *Acknowledgements*. M.B. and T.H. thank the Max Planck Graduate Center with the Johannes Gutenberg-Universität Mainz (MPGC) for financial support. The authors gratefully acknowledge the NOAA Air Resources Laboratory (ARL) for the provision of the HYSPLIT transport and dispersion model and READY website (*http://www.ready.noaa.gov*) used in this publication. Moreover, the authors gratefully acknowledge the Department of Micrometeorology at the University of Bayreuth for providing the RH data.

References

Aiken, A. C., Salcedo, D., Cubison, M. J., Huffman, J. A., DeCarlo, P. F., Ulbrich, I. M., Docherty, K. S., Sueper, D., Kimmel, J. R., Worsnop, D. R., Trimborn, A., Northway, M., Stone, E. A., Schauer, J. J., Volkamer, R. M., Fortner, E., Foy, B. de, Wang, J., Laskin, A., Shutthanandan, V., Zheng, J., Zhang, R., Gaffney, J., Marley, N. A., Paredes-Miranda, G., Arnott, W. P., Molina, L. T., Sosa, G., and Jimenez, J. L.: Mexico City aerosol analysis during MILAGRO using high resolution aerosol mass spectrometry at the urban supersite (T0) – Part 1: Fine particle composition and organic source apportionment, Atmos. Chem. Phys., 9, 6633–6653, doi:10.5194/acp-9-6633-2009, 2009.

Altieri, K. E., Turpin, B. J., and Seitzinger, S. P.: Oligomers, organosulfates, and nitrooxy organosulfates in rainwater identified by ultra-high resolution electrospray ionization FT-ICR mass spectrometry, Atmos. Chem. Phys., 9, 2533–2542, doi:10.5194/acp-9-2533-2009, 2009.

Baltensperger, U., Dommen, J., Alfarra, R.R., Duplissy, J., Gaeggeler, K., Metzger, A., Facchini, M.C.., Decesari, S., Finessi, E., Reinnig, C., Schott, M., Warnke, J., Hoffmann, T., Klatzer, B., Puxbaum, H., Geiser, M., Savi, M., Lang, D., Kalberer, M., and Geiser, T.: Combined Determination of the Chemical Composition and of Health Effects of Secondary Organic Aerosols: The POLYSOA Project, J. Aerosol Med. .Pulm. Drug Deliv. 21, 145-154, doi:10.1089/jamp.2007.0655, 2008.

Brüggemann, M., Karu, E., Stelzer, T., and Hoffmann, T.: Real-Time Analysis of Ambient Organic Aerosols Using Aerosol Flowing Atmospheric-Pressure Afterglow Mass Spectrometry (AeroFAPA-MS), Environ. Sci. Technol., 49, 5571–5578, doi:10.1021/es506186c, 2015.

Canagaratna, M., Jayne, J., Jimenez, J., Allan, J., Alfarra, M., Zhang, Q., Onasch, T., Drewnick, F., Coe, H., Middlebrook, A., Delia, A., Williams, L., Trimborn, A., Northway, M., DeCarlo, P., Kolb, C., Davidovits, P., and Worsnop, D.: Chemical and microphysical characterization of ambient aerosols with the aerodyne aerosol mass spectrometer, Mass Spectrom. Rev., 26, 185–222, doi:10.1002/mas.20115, 2007.

Claeys, M., Iinuma, Y., Szmigielski, R., Surratt, J. D., Blockhuys, F., van Alsenoy, C., Böge, O., Sierau, B., Gómez-González, Y., Vermeylen, R., van der Veken, P., Shahgholi, M., Chan, A. W. H., Herrmann, H., Seinfeld, J. H., and Maenhaut, W.: Terpenylic Acid and Related Compounds from the Oxidation of α-Pinene: Implications for New Particle Formation and Growth above Forests, Environ. Sci. Technol., 43, 6976–6982, doi:10.1021/es9007596, 2009.

Crounse, J. D., Nielsen, L. B., Jørgensen, S., Kjaergaard, H. G., and Wennberg, P. O.: Autoxidation of Organic Compounds in the Atmosphere, J. Phys. Chem. Lett., 4, 3513–3520, doi:10.1021/jz4019207, 2013.

Darer, A. I., Cole-Filipiak, N. C., O'Connor, A. E., and Elrod, M. J.: Formation and Stability of Atmospherically Relevant Isoprene-Derived Organosulfates and Organonitrates, Environ. Sci. Technol., 45, 1895–1902, doi:10.1021/es103797z, 2011.

Donahue, N. M., Kroll, J. H., Pandis, S. N., and Robinson, A. L.: A two-dimensional volatility basis set – Part 2: Diagnostics of organic-aerosol evolution, Atmos. Chem. Phys., 12, 615–634, doi:10.5194/acp-12-615-2012, 2012.

Draxler, R. R. and Rolph, G. D.: HYSPLIT (HYbrid Single-Particle Lagrangian Integrated Trajectory) Model access via NOAA ARL READY Website: http://ready.arl.noaa.gov/HYSPLIT.php, NOAA Air Resources Laboratory, Silver Spring, MD, 2013.

Ehn, M., Kleist, E., Junninen, H., Petäjä, T., Lönn, G., Schobesberger, S., Dal Maso, M., Trimborn, A., Kulmala, M., Worsnop, D. R., Wahner, A., Wildt, J., and Mentel, T. F.: Gas phase formation of extremely oxidized pinene reaction products in chamber and ambient air, Atmos. Chem. Phys., 12, 5113–5127, doi:10.5194/acp-12-5113-2012, 2012.

Ehn, M., Thornton, J. A., Kleist, E., Sipila, M., Junninen, H., Pullinen, I., Springer, M., Rubach, F., Tillmann, R., Lee, B., Lopez-Hilfiker, F., Andres, S., Acir, I.-H., Rissanen, M., Jokinen, T., Schobesberger, S., Kangasluoma, J., Kontkanen, J., Nieminen, T., Kurten, T., Nielsen, L. B., Jørgensen, S., Kjaergaard, H. G., Canagaratna, M., Maso, M. D., Berndt, T., Petaja, T., Wahner, A., Kerminen, V.-M., Kulmala, M., Worsnop, D. R., Wildt, J., and Mentel, T. F.: A large source of low-volatility secondary organic aerosol, Nature, 506, 476–479, 2014.

Farmer, D. K., Matsunaga, A., Docherty, K. S., Surratt, J. D., Seinfeld, J. H., Ziemann, P. J., and Jimenez, J. L.: Response of an aerosol mass spectrometer to organonitrates and organosulfates and implications for atmospheric chemistry, Proceedings of the National Academy of Sciences, 107, 6670–6675, doi:10.1073/pnas.0912340107, 2010.

—

Fushimi, A., Wagai, R., Uchida, M., Hasegawa, S., Takahashi, K., Kondo, M., Hirabayashi, M., Morino, Y., Shibata, Y., Ohara, T., Kobayashi, S., and Tanabe, K.: Radiocarbon (14C) Diurnal Variations in Fine Particles at Sites Downwind from Tokyo, Japan in Summer, Environ. Sci. Technol., 45, 6784–6792, doi:10.1021/es201400p, 2011.

Goldstein, A. H., Koven, C. D., Heald, C. L., and Fung, I. Y.: Biogenic carbon and anthropogenic pollutants combine to form a cooling haze over the southeastern United States, Proceedings of the National Academy of Sciences, 106, 8835–8840, doi:10.1073/pnas.0904128106, 2009.

Guenther, A. B., Jiang, X., Heald, C. L., Sakulyanontvittaya, T., Duhl, T., Emmons, L. K., and Wang, X.: The Model of Emissions of Gases and Aerosols from Nature version 2.1 (MEGAN2.1): an extended and updated framework for modeling biogenic emissions, Geosci. Model Dev., 5, 1471–1492, doi:10.5194/gmd-5-1471-2012, 2012.

Hallquist, M., Wenger, J. C., Baltensperger, U., Rudich, Y., Simpson, D., Claeys, M., Dommen, J., Donahue, N. M., George, C., Goldstein, A. H., Hamilton, J. F., Herrmann, H., Hoffmann, T., Iinuma, Y., Jang, M., Jenkin, M. E., Jimenez, J. L., Kiendler-Scharr, A., Maenhaut, W., McFiggans, G., Mentel, T. F., Monod, A., Prevot, A. S. H., Seinfeld, J. H., Surratt, J. D., Szmigielski, R., and Wildt, J.: The formation, properties and impact of secondary organic aerosol: current and emerging issues, Atmos. Chem. Phys., 9, 5155–5236, 2009.

Held, A., Nowak, A., Birmili, W., Wiedensohler, A., Forkel, R., and Klemm, O.: Observations of particle formation and growth in a mountainous forest region in Central Europe, J. Geophys. Res., 109, 2156–2202, doi:10.1029/2004JD005346, 2004.

Henze, D. K., Seinfeld, J. H., Ng, N. L., Kroll, J. H., Fu, T.-M., Jacob, D. J., and Heald, C. L.: Global modeling of secondary organic aerosol formation from aromatic hydrocarbons: high- vs. low-yield pathways, Atmos. Chem. Phys., 8, 2405–2420, doi:10.5194/acp-8-2405-2008, 2008.

Herrmann, H., Schaefer, T., Tilgner, A., Styler, S. A., Weller, C., Teich, M., and Otto, T.: Tropospheric Aqueous-Phase Chemistry: Kinetics, Mechanisms, and Its Coupling to a Changing Gas Phase, Chem. Rev., 115, 4259–4334, doi:10.1021/cr500447k, 2015.

Hoffmann, T., Bandur, R., Marggraf U., and Linscheid M.: Molecular composition of organic aerosols formed in the alpha-pinene/O3 reaction: Implications for new particle formation processes, Geophys. Res. Lett., 103, 25569–25578, 1998.

Iinuma, Y., Böge, O., Miao, Y., Sierau, B., Gnauk, T., and Herrmann, H.: Laboratory studies on secondary organic aerosol formation from terpenes, Faraday Discuss., 130, 279–294, doi:10.1039/B502160J, 2005.

Iinuma, Y., Müller, C., Berndt, T., Böge, O., Claeys, M., and Herrmann, H.: Evidence for the Existence of Organosulfates from β-Pinene Ozonolysis in Ambient Secondary Organic Aerosol, Environ. Sci. Technol., 41, 6678–6683, doi:10.1021/es070938t, 2007.

Iinuma, Y., Keywood, M., Gnauk, T., and Herrmann, H.: Diaterebic Acid Acetate and Diaterpenylic Acid Acetate: Atmospheric Tracers for Secondary Organic Aerosol Formation from 1,8-Cineole Oxidation, Environ. Sci. Technol., 43, 280–285, doi:10.1021/es802141v, 2009.

Intergovernmental Panel on Climate Change (Ed.): Climate Change 2013 - The Physical Science Basis, Cambridge University Press, Cambridge, 2014.

Jaoui, M., Corse, E., Kleindienst, T. E., Offenberg, J. H., Lewandowski, M., and Edney, E. O.: Analysis of Secondary Organic Aerosol Compounds from the Photooxidation of d -Limonene in the Presence of NOX and their Detection in Ambient PM 2.5, Environ. Sci. Technol., 40, 3819–3828, doi:10.1021/es052566z, 2006.

Jokinen, T., Berndt, T., Makkonen, R., Kerminen, V.-M., Junninen, H., Paasonen, P., Stratmann, F., Herrmann, H., Guenther, A. B., Worsnop, D. R., Kulmala, M., Ehn, M., and Sipilä, M.: Production of extremely low volatile organic compounds from biogenic emissions: Measured yields and atmospheric implications, Proceedings of the National Academy of Sciences, 112, 7123–7128, doi:10.1073/pnas.1423977112, 2015.

Jokinen, T., Sipilä, M., Junninen, H., Ehn, M., Lönn, G., Hakala, J., Petäjä, T., Mauldin III, R. L., Kulmala, M., and Worsnop, D. R.: Atmospheric sulphuric acid and neutral cluster measurements using CI-APi-TOF, Atmos. Chem. Phys., 12, 4117–4125, doi:10.5194/acp-12-4117-2012, 2012.

Jokinen, T., Sipilä, M., Richters, S., Kerminen, V.-M., Paasonen, P., Stratmann, F., Worsnop, D., Kulmala, M., Ehn, M., Herrmann, H., and Berndt, T.: Rapid Autoxidation Forms Highly Oxidized RO2 Radicals in the Atmosphere, Angew. Chem. Int. Ed., 53, 14596–14600, doi:10.1002/anie.201408566, 2014.

Kolb, C. E., Cox, R. A., Abbatt, J. P. D., Ammann, M., Davis, E. J., Donaldson, D. J., Garrett, B. C., George, C., Griffiths, P. T., Hanson, D. R., Kulmala, M., McFiggans, G., Pöschl, U., Riipinen, I., Rossi, M. J., Rudich, Y., Wagner, P. E.,

Winkler, P. M., Worsnop, D. R., and O' Dowd, C. D.: An overview of current issues in the uptake of atmospheric trace gases by aerosols and clouds, Atmos. Chem. Phys., 10, 10561–10605, doi:10.5194/acp-10-10561-2010, 2010.

Kristensen, K., and Glasius, M.: Organosulfates and oxidation products from biogenic hydrocarbons in fine aerosols from a forest in North West Europe during spring, Atmos. Env., 45, 4546–4556, doi:10.1016/j.atmosenv.2011.05.063, 2011.

5 Liggio, J. and Li, S.-M.: Organosulfate formation during the uptake of pinonaldehyde on acidic sulfate aerosols, Geophys. Res. Lett., 33, n/a, doi:10.1029/2006GL026079, 2006.

Lin, P., Yu, J. Z., Engling, G., and Kalberer, M.: Organosulfates in Humic-like Substance Fraction Isolated from Aerosols at Seven Locations in East Asia: A Study by Ultra-High-Resolution Mass Spectrometry, Environ. Sci. Technol., 46, 13118–13127, doi:10.1021/es303570v, 2012.

10 Mentel, T. F., Springer, M., Ehn, M., Kleist, E., Pullinen, I., Kurtén, T., Rissanen, M., Wahner, A., and Wildt, J.: Formation of highly oxidized multifunctional compounds: autoxidation of peroxy radicals formed in the ozonolysis of alkenes – deduced from structure–product relationships, Atmos. Chem. Phys., 15, 6745–6765, doi:10.5194/acp-15-6745-2015, 2015.

Middlebrook, A. M., Bahreini, R., Jimenez, J. L., and Canagaratna, M. R.: Evaluation of Composition-Dependent Collection

15 Efficiencies for the Aerodyne Aerosol Mass Spectrometer using Field Data, Aerosol Science and Technology, 46, 258–271, doi:10.1080/02786826.2011.620041, 2012.

Müller, L., Reinnig, M.-C., Naumann, K. H., Saathoff, H., Mentel, T. F., Donahue, N. M., and Hoffmann, T.: Formation of 3-methyl-1,2,3-butanetricarboxylic acid via gas phase oxidation of pinonic acid – a mass spectrometric study of SOA aging, Atmos. Chem. Phys., 12, 1483–1496, doi:10.5194/acp-12-1483-2012, 2012.

20 Mutzel, A., Poulain, L., Berndt, T., Iinuma, Y., Rodigast, M., Böge, O., Richters, S., Spindler, G., Sipilä, M., Jokinen, T., Kulmala, M., and Herrmann, H.: Highly Oxidized Multifunctional Organic Compounds Observed in Tropospheric Particles: A Field and Laboratory Study, Environ. Sci. Technol., 49, 7754–7761, doi:10.1021/acs.est.5b00885, 2015.

Nguyen, T. B., Lee, P. B., Updyke, K. M., Bones, D. L., Laskin, J., Laskin, A., and Nizkorodov, S. A.: Formation of nitrogen- and sulfur-containing light-absorbing compounds accelerated by evaporation of water from secondary organic

25 aerosols, J. Geophys. Res., 117, doi:10.1029/2011JD016944, 2012.

Nozière, B., Ekström, S., Alsberg, T., and Holmström, S.: Radical-initiated formation of organosulfates and surfactants in atmospheric aerosols, Geophys. Res. Lett., 37, n/a, doi:10.1029/2009GL041683, 2010.

Nozière, B., Kalberer, M., Claeys, M., Allan, J., D'Anna, B., Decesari, S., Finessi, E., Glasius, M., Grgić, I., Hamilton, J. F., Hoffmann, T., Iinuma, Y., Jaoui, M., Kahnt, A., Kampf, C. J., Kourtchev, I., Maenhaut, W., Marsden, N., Saarikoski, S.,

30 Schnelle-Kreis, J., Surratt, J. D., Szidat, S., Szmigielski, R., and Wisthaler, A.: The Molecular Identification of Organic Compounds in the Atmosphere: State of the Art and Challenges, Chem. Rev., doi:10.1021/cr5003485, 2015.

Pöschl, U.: Atmospheric aerosols: Composition, transformation, climate and health effects, Angew. Chem. Int. Edit., 44, 7520–7540, doi:10.1002/anie.200501122, 2005.

Poulain, L., Birmili, W., Canonaco, F., Crippa, M., Wu, Z. J., Nordmann, S., Spindler, G., Prévôt, A. S. H., Wiedensohler,

35 A., and Herrmann, H.: Chemical mass balance of 300 °C non-volatile particles at the tropospheric research site Melpitz, Germany, Atmos. Chem. Phys., 14, 10145–10162, doi:10.5194/acp-14-10145-2014, 2014.

Riipinen, I., Pierce, J. R., Yli-Juuti, T., Nieminen, T., Häkkinen, S., Ehn, M., Junninen, H., Lehtipalo, K., Petäjä, T., Slowik, J., Chang, R., Shantz, N. C., Abbatt, J., Leaitch, W. R., Kerminen, V.-M., Worsnop, D. R., Pandis, S. N., Donahue, N. M., and Kulmala, M.: Organic condensation: a vital link connecting aerosol formation to cloud condensation nuclei

40 (CCN) concentrations, Atmos. Chem. Phys., 11, 3865–3878, doi:10.5194/acp-11-3865-2011, 2011.

Rissanen, M. P., Kurtén, T., Sipilä, M., Thornton, J. A., Kangasluoma, J., Sarnela, N., Junninen, H., Jørgensen, S., Schallhart, S., Kajos, M. K., Taipale, R., Springer, M., Mentel, T. F., Ruuskanen, T., Petäjä, T., Worsnop, D. R., Kjaergaard, H. G., and Ehn, M.: The Formation of Highly Oxidized Multifunctional Products in the Ozonolysis of Cyclohexene, J. Am. Chem. Soc., 136, 15596–15606, doi:10.1021/ja507146s, 2014.

45 Seinfeld, J. and Pandis, S.: Atmospheric chemistry and physics: from air pollution to climate change, Wiley, 2006.

Shang, J., Passananti, M., Dupart, Y., Ciuraru, R., Tinel, L., Rossignol, S., Perrier, S., Zhu, T. and George, C.: SO$_2$ Uptake on Oleic Acid: A New Formation Pathway of Organosulfur Compounds in the Atmosphere, Environmental Science & Technology Letters Environ. Sci. Technol. Lett., 3(2), 67–72, doi:10.1021/acs.estlett.6b00006, 2016.

Shiraiwa, M., Zuend, A., Bertram, A. K., and Seinfeld, J. H.: Gas–particle partitioning of atmospheric aerosols: interplay of

50 physical state, non-ideal mixing and morphology, Phys. Chem. Chem. Phys., 15, 11441, doi:10.1039/c3cp51595h, 2013.

Staudt, K., Foken, T.: Documentation of reference data for the experimental areas of the Bayreuth Centre for Ecology and Environmental Research (BayCEER) at the Waldstein site, Arbeitsergebnisse, Universität Bayreuth, Mikrometeorologie (ISSN 1614-8916), 35, 1–35, 2007.

Surratt, J. D., Gómez-González, Y., Chan, A. W. H., Vermeylen, R., Shahgholi, M., Kleindienst, T. E., Edney, E. O., Offenberg, J. H., Lewandowski, M., Jaoui, M., Maenhaut, W., Claeys, M., Flagan, R. C., and Seinfeld, J. H.: Organosulfate Formation in Biogenic Secondary Organic Aerosol, J. Phys. Chem. A, 112, 8345–8378, doi:10.1021/jp802310p, 2008.

Surratt, J. D., Kroll, J. H., Kleindienst, T. E., Edney, E. O., Claeys, M., Sorooshian, A., Ng, N. L., Offenberg, J. H., Lewandowski, M., Jaoui, M., Flagan, R. C., and Seinfeld, J. H.: Evidence for Organosulfates in Secondary Organic Aerosol, Environ. Sci. Technol., 41, 517–527, doi:10.1021/es062081q, 2007.

Szmigielski, R., Surratt, J. D., Vermeylen, R., Szmigielska, K., Kroll, J. H., Ng, N. L., Murphy, S. M., Sorooshian, A., Seinfeld, J. H., and Claeys, M.: Characterization of 2-methylglyceric acid oligomers in secondary organic aerosol formed from the photooxidation of isoprene using trimethylsilylation and gas chromatography/ion trap mass spectrometry, Journal of Mass Spectrometry, 42, 101–116, doi:10.1002/jms.1146, 2007.

Tröstl, J., Chuang, W. K., Gordon, H., Heinritzi, M., Yan, C., Molteni, U., Ahlm, L., Frege, C., Bianchi, F., Wagner, R., Simon, M., Lehtipalo, K., Williamson, C., Craven, J. S., Duplissy, J., Adamov, A., Almeida, J., Bernhammer, A.-K., Breitenlechner, M., Brilke, S., Dias, A., Ehrhart, S., Flagan, R. C., Franchin, A., Fuchs, C., Guida, R., Gysel, M., Hansel, A., Hoyle, C. R., Jokinen, T., Junninen, H., Kangasluoma, J., Keskinen, H., Kim, J., Krapf, M., Kürten, A., Laaksonen, A., Lawler, M., Leiminger, M., Mathot, S., Möhler, O., Nieminen, T., Onnela, A., Petäjä, T., Piel, F. M., Miettinen, P., Rissanen, M. P., Rondo, L., Sarnela, N., Schobesberger, S., Sengupta, K., Sipilä, M., Smith, J. N., Steiner, G., Tomè, A., Virtanen, A., Wagner, A. C., Weingartner, E., Wimmer, D., Winkler, P. M., Ye, P., Carslaw, K. S., Curtius, J., Dommen, J., Kirkby, J., Kulmala, M., Riipinen, I., Worsnop, D. R., Donahue, N. M. and Baltensperger, U.: The role of low-volatility organic compounds in initial particle growth in the atmosphere, Nature, 533(7604), 527–531, doi:10.1038/nature18271, 2016.

van Eijck, A., Opatz, T., Taraborrelli, D., Sander, R., and Hoffmann, T.: New tracer compounds for secondary organic aerosol formation from β-caryophyllene oxidation, Atmospheric Environment, 80, 122 – 130, doi: 10.1016/j.atmosenv.2013.07.060, 2013.

Wiedensohler, A., Birmili, W., Nowak, A., Sonntag, A., Weinhold, K., Merkel, M., Wehner, B., Tuch, T., Pfeifer, S., Fiebig, M., Fjäraa, A. M., Asmi, E., Sellegri, K., Depuy, R., Venzac, H., Villani, P., Laj, P., Aalto, P., Ogren, J. A., Swietlicki, E., Williams, P., Roldin, P., Quincey, P., Hüglin, C., Fierz-Schmidhauser, R., Gysel, M., Weingartner, E., Riccobono, F., Santos, S., Grüning, C., Faloon, K., Beddows, D., Harrison, R., Monahan, C., Jennings, S. G., O'Dowd, C. D., Marinoni, A., Horn, H.-G., Keck, L., Jiang, J., Scheckman, J., McMurry, P. H., Deng, Z., Zhao, C. S., Moerman, M., Henzing, B., Leeuw, G. de, Löschau, G., and Bastian, S.: Mobility particle size spectrometers: harmonization of technical standards and data structure to facilitate high quality long-term observations of atmospheric particle number size distributions, Atmos. Meas. Tech., 5, 657–685, doi:10.5194/amt-5-657-2012, 2012.

Yasmeen, F., Szmigielski, R., Vermeylen, R., Gómez-González, Y., Surratt, J. D., Chan, A. W. H., Seinfeld, J. H., Maenhaut, W., and Claeys, M.: Mass spectrometric characterization of isomeric terpenoic acids from the oxidation of α-pinene, β-pinene, d-limonene, and Δ3-carene in fine forest aerosol, J. Mass. Spectrom., 46, 425–442, doi:10.1002/jms.1911, 2011.

Yatavelli, R. L. N., Mohr, C., Stark, H., Day, D. A., Thompson, S. L., Lopez-Hilfiker, F. D., Campuzano-Jost, P., Palm, B. B., Vogel, A. L., Hoffmann, T., Heikkinen, L., Äijälä, M., Ng, N. L., Kimmel, J. R., Canagaratna, M. R., Ehn, M., Junninen, H., Cubison, M. J., Petäjä, T., Kulmala, M., Jayne, J. T., Worsnop, D. R., and Jimenez, J. L.: Estimating the contribution of organic acids to northern hemispheric continental organic aerosol, Geophys. Res. Lett., 42, 6084–6090, doi:10.1002/2015GL064650, 2015.

Yu, J., Flagan, R. C., and Seinfeld, J. H.: Identification of Products Containing −COOH, −OH, and −CO in Atmospheric Oxidation of Hydrocarbons, Environ. Sci. Technol., 32, 2357–2370, doi:10.1021/es980129x, 1998.

Zhang, R., Wang, L., Khalizov, A. F., Zhao, J., Zheng, J., McGraw, R. L., and Molina, L. T.: Formation of nanoparticles of blue haze enhanced by anthropogenic pollution, Proceedings of the National Academy of Sciences, 106, 17650–17654, doi:10.1073/pnas.0910125106, 2009.

Zhao, J., Ortega, J., Chen, M., McMurry, P. H., and Smith, J. N.: Dependence of particle nucleation and growth on high-molecular-weight gas-phase products during ozonolysis of α-pinene, Atmos. Chem. Phys., 13, 7631–7644, doi:10.5194/acp-13-7631-2013, 2013.

Table 1. Common BSOA marker compounds which were identified among the CHO compounds. The average concentrations were determined using pinic acid as reference. Standard deviations are given in brackets. A complete list of all identified CHO compounds can be found in the Supplemental Material.

formula for $[M–H]^-$	measured m/z	assigned compound	average conc. / ng m^{-3}
$C_8H_{11}O_4$	171.0663	terpenylic acid	6.4 ($\pm$ 3.8)
$C_8H_{11}O_5$	187.0612	2-hydroxyterpenylic acid	7.7 ($\pm$ 5.0)
$C_8H_{11}O_6$ [a]	203.0561	MBTCA	13.8 ($\pm$ 9.0)
		3-carboxyheptanedioic acid	10.2 ($\pm$ 6.6)
$C_9H_{13}O_4$	185.0819	pinic acid	4.7 ($\pm$ 2.5)
$C_{10}H_{15}O_6$	231.0874	diaterpenylic acid acetate	5.2 ($\pm$ 2.7)
$C_{13}H_{19}O_5$	255.1238	β-nocaryophillinic acid	– [b]
$C_{17}H_{25}O_8$	357.1555	pinyl-diaterpenylic ester	– [b]

[a] isobaric compounds; [b] below quantification limit

Table 2. Identified highly oxidized organosulfates (HOOS) by LC–MS from filter sample extracts. A comprehensive list of all detected sulfur- and nitrogen-containing compounds is given in the Supplemental Material.

formula for $[M–H]^-$	measured m/z	Δm / ppm	O:C
$C_7H_{11}O_7S$	239.0231	0.0	1.0
$C_7H_{13}O_7S$	241.0385	-1.0	1.0
$C_7H_7O_8S$	250.9868	0.3	1.1
$C_7H_9O_8S$	253.0028	1.7	1.1
$C_8H_{11}O_9S$	283.0127	-0.8	1.1
$C_8H_{13}O_9S$	285.0284	-0.6	1.1
$C_8H_{13}O_{10}S$	301.0231	-1.3	1.3
$C_9H_{13}O_8S$	281.0334	-0.9	0.9
$C_9H_{13}O_9S$	297.0282	-1.3	1.0
$C_{10}H_{15}O_{10}S$	327.0387	-1.4	1.0
$C_{10}H_{13}O_{11}S$	341.0183	-0.3	1.1
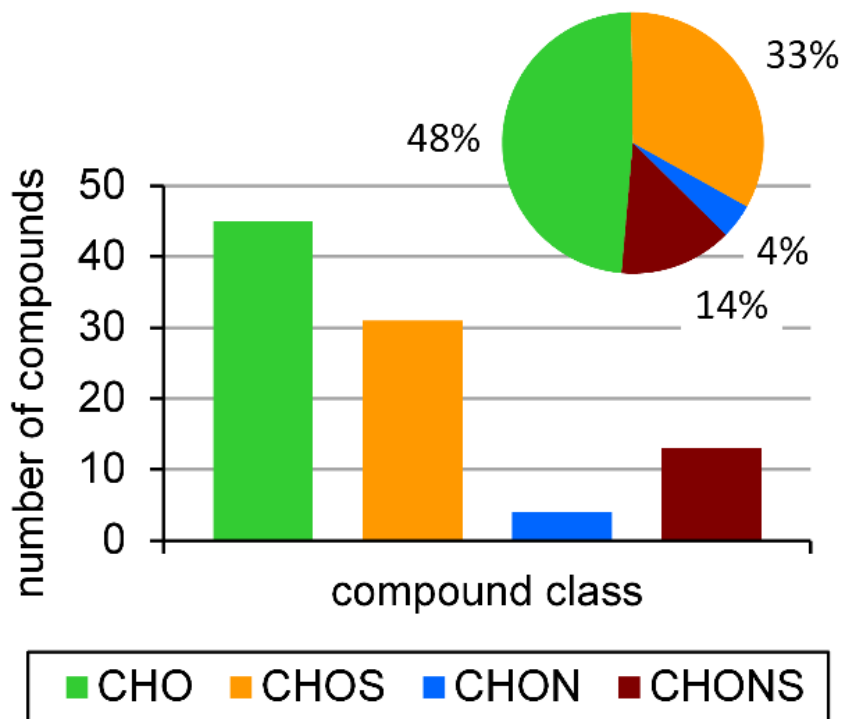
Figure 1. Number and fraction of identified compounds by LC–MS analysis of filter sample extracts for each compound class.
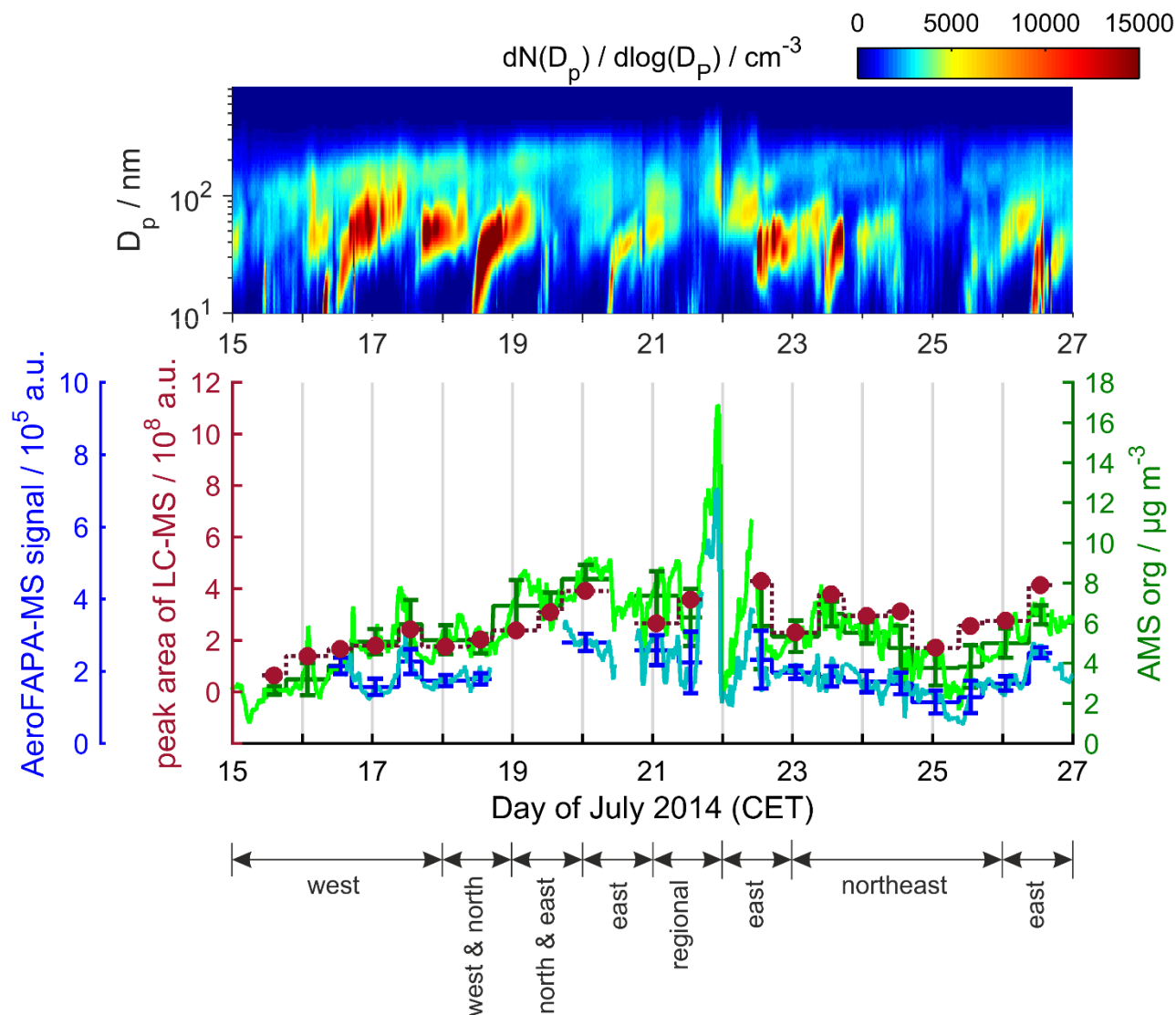
Figure 2. Top panel: Number size distribution of aerosol particles which was measured by the SMPS. Middle panel: Sum of the peak areas for the 93 identified compounds from the filter samples by LC–HRMS (red). The signals for these compounds, measured by AeroFAPA–MS (blue), and the organic aerosol mass, measured by an AMS (green), show similar trends. Averaged values for the filter sampling times are depicted by the horizontal lines (errorbars show one standard deviation). Bottom panel: Major source directions of 96 hours backward trajectories arriving at the site (250 m above ground level).
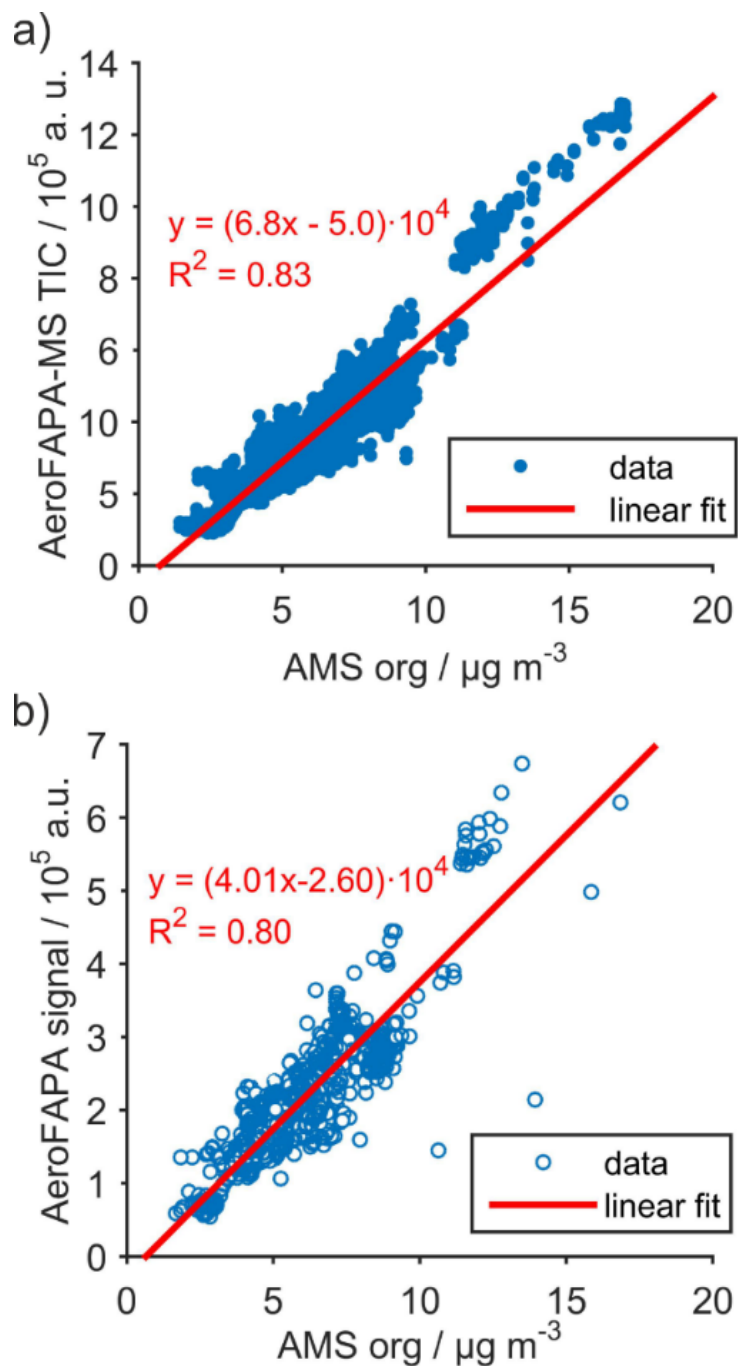
Figure 3. Correlation between organic aerosol mass (AMS org) and AeroFAPA–MS signals. (a) Total ion current of AeroFAPA as function of organic aerosol mass (blue dots) and linear fit (red line). (b) AeroFAPA–MS signals for compounds, that were identified by LC–MS analysis of filter samples, as a function of organic aerosol mass (blue circles) and linear fit (red line).
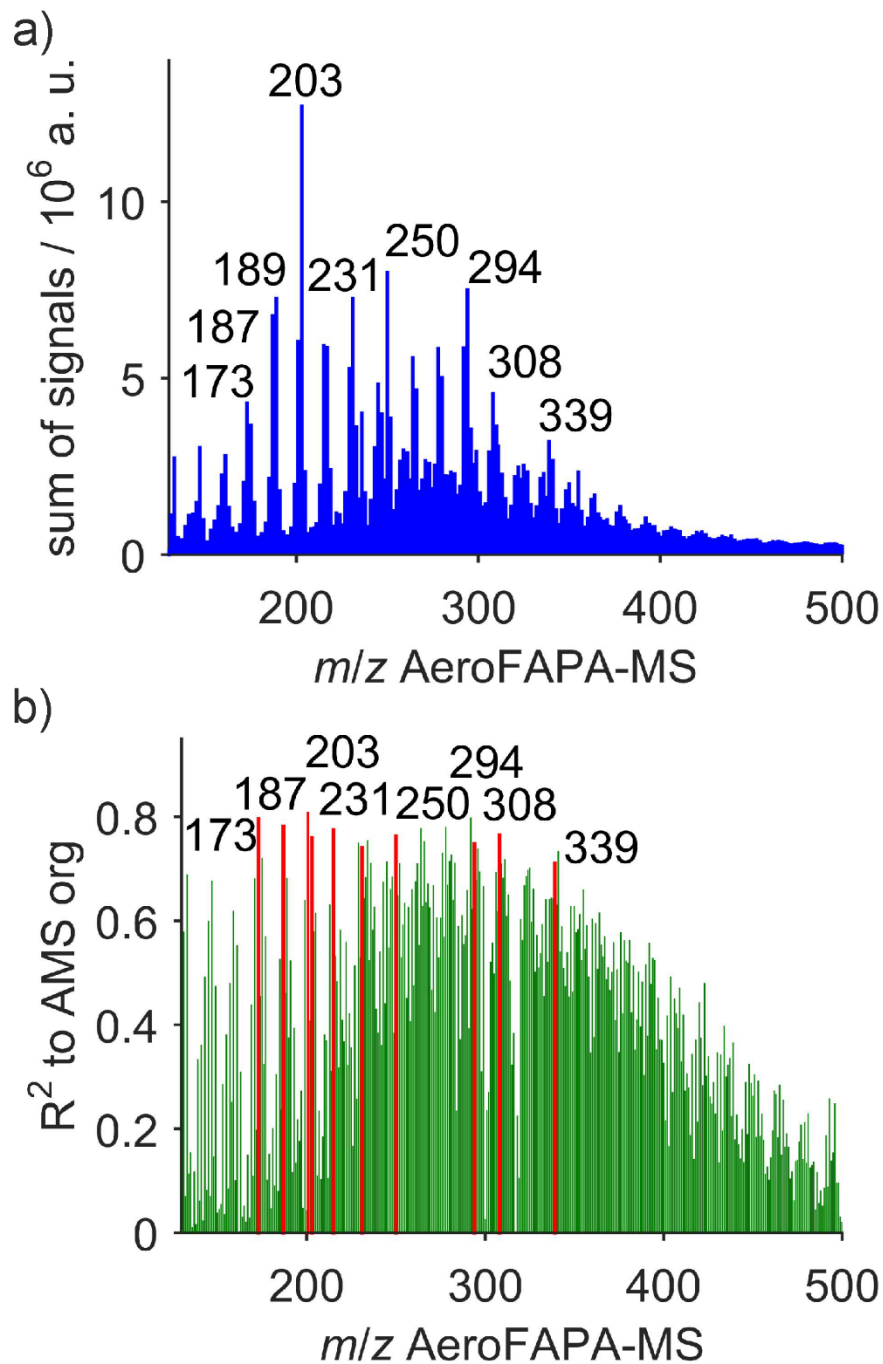
Figure 4. (a) Sum of signals during the campaign period of the AeroFAPA–MS. (b) Linear correlations between m/z ratios of AeroFAPA–MS and total organic aerosol mass measured by the AMS.
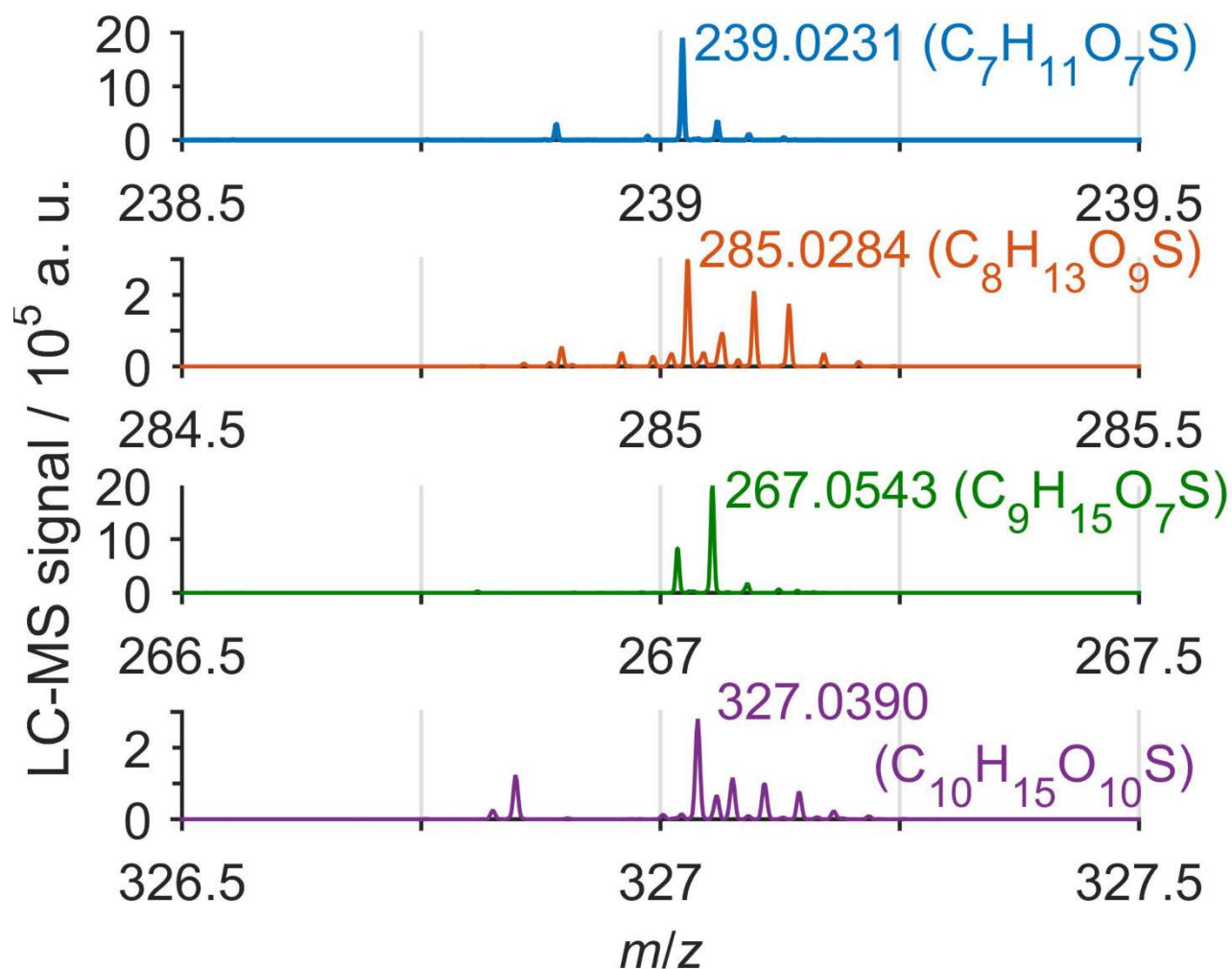
Figure 5. Mass spectra of the LC–MS analysis of a filter sample (mass resolution of R=7·10⁴ at *m/z* 200). Four HOOS compounds were chosen as representative according to their number of carbon atoms (C₇–C₁₀) and signal abundance.
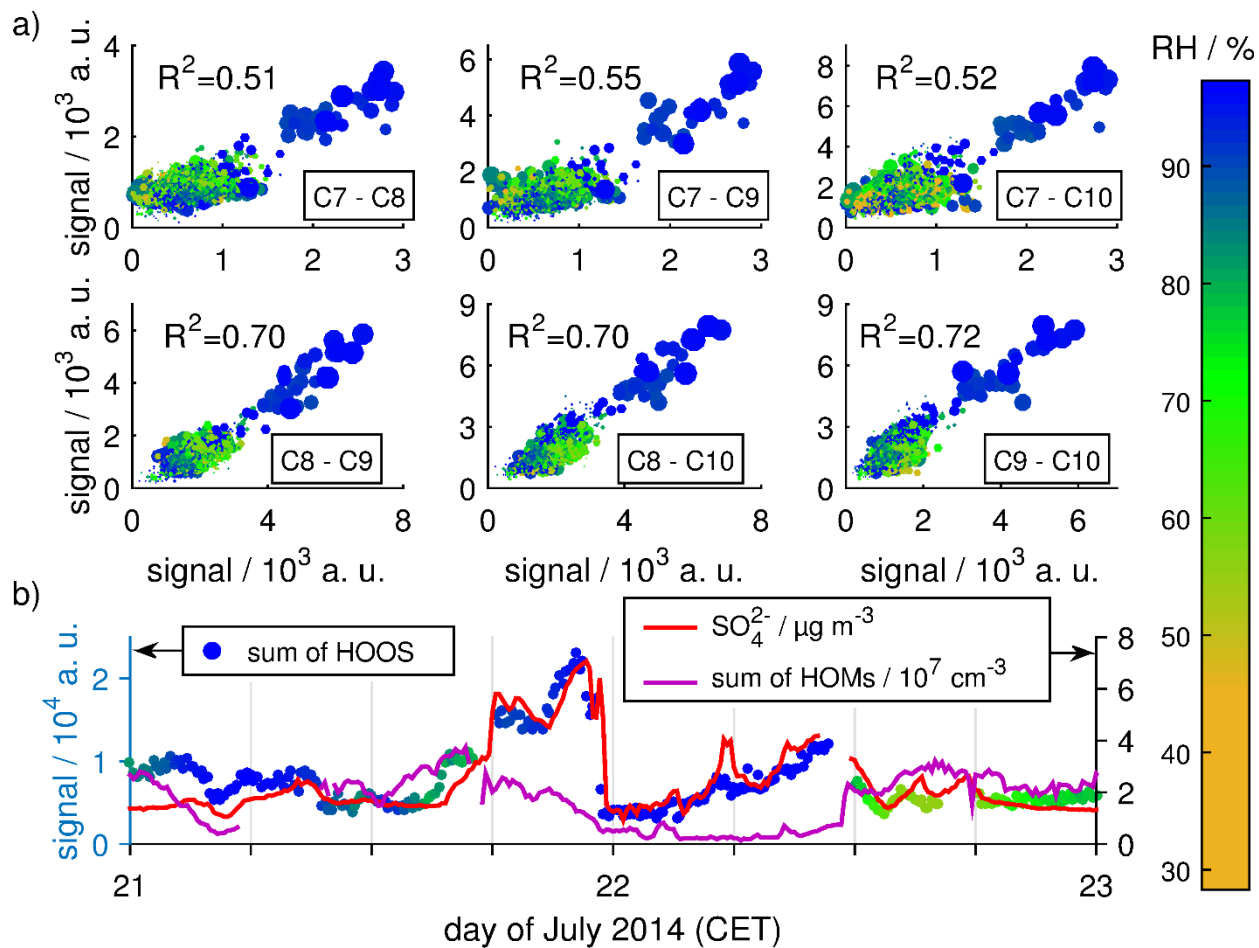
Figure 6. (a) Correlations among the HOOS classes and effect of RH (color code) and particulate sulfate on their formation (marker size, range: 0.8–7.2 µg·m⁻³). (b) Comparison of the sum of HOOS signals, particulate sulfate, and sum concentration of gas-phase HOMs during July 21ˢᵗ–23ʳᵈ, demonstrating good agreement between HOOS and sulfate for high RH periods.
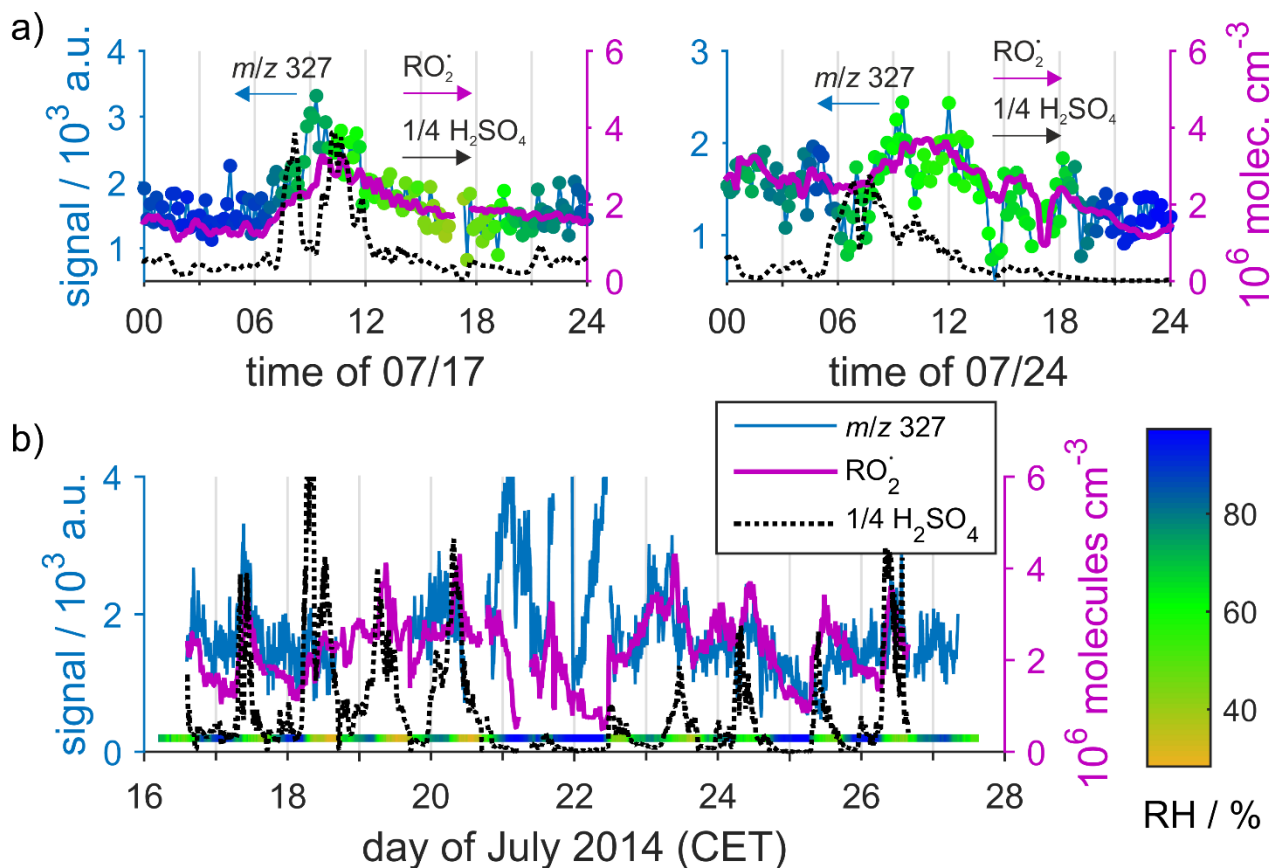
Figure 7. Signals for C10 HOOS (*m/z* 327), gas-phase H_2SO_4, $RO_2^\bullet$ ($C_{10}H_{15}O_8^\bullet$), and RH. (a) Time traces for the signals for July 17th and 24th, showing good agreement between C10 HOOS and $RO_2^\bullet$. (b) Time traces for the entire campaign period, demonstrating the influence of RH on HOOS formation and $RO_2^\bullet$ abundance. For better visibility the HOOS signal is allowed to go off scale for July 21st and 22nd.